

# Cosmic voids in coupled dark energy cosmologies: the impact of halo bias

Giorgia Pollina<sup>1,4,5</sup>, Marco Baldi<sup>1,2,3</sup>, Federico Marulli<sup>1,2,3</sup>, Lauro Moscardini<sup>1,2,3</sup>

<sup>1</sup>Dipartimento di Fisica e Astronomia, Alma Mater Studiorum Università di Bologna, viale Berti Pichat, 6/2, I-40127 Bologna, Italy

<sup>2</sup>INAF - Osservatorio Astronomico di Bologna, via Ranzani 1, I-40127 Bologna, Italy

<sup>3</sup>INFN - Sezione di Bologna, viale Berti Pichat 6/2, I-40127 Bologna, Italy

<sup>4</sup>Universitäts-Sternwarte München, Fakultät für Physik, Ludwig-Maximilians Universität München, Scheinerstr. 1, D-81679 München, Germany

<sup>5</sup>Excellence Cluster Universe, Boltzmannstr. 2, D-85748 Garching, Germany

31 August 2018

## ABSTRACT

In this work we analyse the properties of cosmic voids in standard and coupled dark energy cosmologies. Using large numerical simulations, we investigate the effects produced by the dark energy coupling on three statistics: the filling factor, the size distribution and the stacked profiles of cosmic voids. We find that the bias of the tracers of the density field used to identify the voids strongly influences the properties of the void catalogues, and, consequently, the possibility of using the identified voids as a probe to distinguish coupled dark energy models from the standard  $\Lambda$ CDM cosmology. In fact, on one hand coupled dark energy models are characterised by an excess of large voids in the cold dark matter distribution as compared to the reference standard cosmology, due to their higher normalisation of linear perturbations at low redshifts. Specifically, these models present an excess of large voids with  $R_{\text{eff}} > 20, 15, 12 h^{-1} \text{Mpc}$ , at  $z = 0, 0.55, 1$ , respectively. On the other hand, we do not find any significant difference in the properties of the voids detected in the distribution of collapsed dark matter halos. These results imply that the tracer bias has a significant impact on the possibility of using cosmic void catalogues to probe cosmology.

**Key words:** dark energy – dark matter – cosmology: theory – galaxies: formation

## 1 INTRODUCTION

Despite the fact that the presently accepted standard cosmological model, the so-called  $\Lambda$ CDM scenario, appears to be fully consistent with most of the available observations (see e.g. Planck Collaboration et al. 2015a), it still presents some open issues in the detailed description of the distribution of matter at small scales. One of such properties that still appears problematic is the observed abundance of dwarf galaxies in the underdense regions of the Universe, which is found to be significantly lower than what predicted by large N-body simulations carried out within the  $\Lambda$ CDM cosmology. This problem, that was pointed out for the first time by Peebles (2001), goes under the name of the *void phenomenon*, and it has been discussed by several authors over the past years (see e.g. Tinker & Conroy 2009; Sutter et al. 2015a).

Besides the poor theoretical understanding of a cosmological constant as source of the observed accelerated expansion of the Universe (Weinberg 1989), the void phenomenon is therefore one of the few observational tensions that motivate the investigation of alternative cosmological scenarios, together with the so-called *cusp-core problem* (de Blok 2010), the *satellite problem* (Bullock 2010), the *too big to fail problem* (Boylan-Kolchin, Bullock & Kaplinghat 2011), and the recently

detected tension between the CMB- and cluster-based estimations of  $\sigma_8$ , the r.m.s. of the mass density field within a sphere of radius  $8 h^{-1} \text{Mpc}$  (Planck Collaboration et al. 2015b).

A relevant class of alternative cosmological models that has been widely investigated in recent years is given by the so-called coupled dark energy scenario (cDE hereafter, see e.g. Wetterich 1995; Amendola 2000, 2004; Farrar & Peebles 2004; Baldi 2011b). In these models a dynamical scalar field sourcing the accelerated cosmic expansion (see e.g. Wetterich 1988; Ratra & Peebles 1988) is coupled to cold dark matter (CDM) particles resulting in a direct exchange of energy-momentum between these two cosmic components. Such interaction gives rise to a new fifth force acting on CDM particles, possibly capable to make the voids emptier (Nusser, Gubser & Peebles 2005). Other possible ways to address the void phenomenon have been proposed, such as, for example, a modification of gravity at very large scales (Li & Zhao 2009; Clampitt, Cai & Li 2013; Spolyar, Sahlén & Silk 2013).

The main effects of cDE models on the large-scale matter distribution in the Universe, as well as on the structural properties of highly nonlinear collapsed objects (such as galaxies and galaxy clusters), have been widely investigated in the recent past by several works mostly based on dedicated large N-body simulations (see

e.g. Macciò et al. 2004; Baldi et al. 2010; Li & Barrow 2011; Baldi 2011a, 2012b; Cervantes et al. 2012; Marulli, Baldi & Moscardini 2012; Giocoli et al. 2013; Moresco et al. 2014; Carlesi et al. 2014a,b). However, in these rich and high-dense environments the effects produced by cDE are expected to be significantly modified by the complex and not yet fully understood baryonic processes occurring within astrophysical objects. Therefore, studying the properties of underdense regions of the universe might represent a complementary approach to investigate cDE scenarios, and might provide a direct test of such cosmological models through a direct comparison with the properties of the observed cosmic voids (hereafter CV).

Although the existence of CV - defined as large underdense regions of the Universe - was one of the earliest predictions of the standard cosmological model (Hausman, Olson & Roth 1983), and the observational discovery of CV dates back to over than 30 years ago (see Gregory, Thompson & Tifft 1978; Kirshner et al. 1981), it is only in recent years that systematic studies about CV have become possible thanks to the increasing depth and volume of current galaxy surveys and to the advent of large numerical simulations that allow to predict with high accuracy the topology of the cosmic web.

The recent interest for CV is mostly related to their yet unexploited potential to probe cosmological models and constrain cosmological parameters, thanks to the claimed universality of their general statistical and structural properties (see e.g. Colberg et al. 2005; Ricciardelli, Quilis & Planelles 2013; Ricciardelli, Quilis & Varela 2014). In particular, CV might represent a population of ideal spheres with a homogeneous distribution in the Universe at different redshifts, so that their size evolution can be used to characterise the expansion history of the Universe by means of the Alcock & Paczynski (AP) test (Alcock & Paczynski 1979), as already pointed out by recent works (Sutter et al. 2012, 2014).

Furthermore, CV might have an impact on the observed properties of the Cosmic Microwave Background (CMB), and the persisting CMB anomalies like the Cold Spot could be explained as resulting from the Integrated Sachs-Wolfe effect over large CV, as suggested by different works (Rees, Sciama & Stobbs 1968; Szapudi et al. 2014; Kovač et al. 2014; Finelli et al. 2014). The next generation of large galaxies surveys such as the ESA Euclid mission (Laureijs et al. 2011; Amendola et al. 2013) are expected to detect gravitational lensing from medium size CV with which it will be possible to directly constrain the void density profiles without resorting on luminous tracers like galaxies, which would require to model their bias (Izumi et al. 2013; Krause et al. 2013; Melchior et al. 2014; Clampitt & Jain 2014).

CV are therefore one of the most appealing and promising cosmological probes: being almost empty, their growth during the cosmic history should be at most weakly nonlinear and their properties could be possibly affected by the nature of DE and by the properties of the primordial density field in which they evolve (Odrzywołek 2009; D'Amico et al. 2011; Bos et al. 2012; Gibbons et al. 2014). In particular, the shape of CV has been shown to be very sensitive to the equation of state of the DE component (Lavaux & Wandelt 2010). Defining the properties of CV in different cosmological models can then represent an important handle to discriminate between these models.

The present work focuses on the investigation of the properties of CV in the standard  $\Lambda$ CDM cosmology, as well as in a series of competing cDE models. This has been done by extracting the population of CV from both the cold dark matter (CDM) and the halo distributions arising in large cosmological N-body

simulations of these different cosmological scenarios. To this end, we made use of the publicly available data of the CoDECS simulations (Baldi 2012c), including three different models of DE interaction besides a  $\Lambda$ CDM reference run. We identified CV in the CoDECS runs with VIDE (Void IDentification and Examination toolkit, Sutter et al. 2015c), a substantially modified version of the publicly-available void finder ZOBOV (ZOnes Bordering On Voidness, Neyrinck 2008), and compared the statistical and structural properties of the resulting void catalogs. Our results show that cDE models are characterised by an excess of large CV in the CDM distribution with respect to the reference  $\Lambda$ CDM cosmology, as expected from their higher normalisation of linear perturbations at low redshifts. This is consistent with the theoretical predictions on the abundance of CV presented in Pisani et al. (2015), while the latter work seems to be in contrast with the recent findings of Sutter et al. (2015b) for the case of coupled dark energy simulations normalised to the same perturbations amplitude.

Nonetheless, we also found that the differences in the CV properties among these different models significantly change when the CV are identified in the distribution of collapsed halos rather than in the CDM distribution itself. These results suggest that, contrary to what has been claimed in some other recent works (see e.g. Sutter et al. 2015a), the bias of the tracers of the density field employed to identify the CV might have a significant impact on the possibility of using the obtained CV catalogs to probe cosmology. Therefore, in the present work we will show that a random subsampling of a simulated CDM distribution to match the density of tracers expected for any given galaxy survey does not actually provide a faithful representation of the discriminating power of the survey with respect to different competing cosmological models.

The paper is organised as follows. In Section 2 we briefly describe the cDE models considered in the present work and we recall the main features of the CoDECS runs. In Section 3 we describe the void finder algorithm and our method of analysis, and in Section 4 we present the properties of the CV in the CoDECS simulations. Our conclusions are summarised in Section 5.

## 2 COUPLED DARK ENERGY COSMOLOGIES

### 2.1 The models

In this work we aim at studying the statistical and structural properties of CV in the context of coupled dark energy (cDE) cosmologies. In these models, dark energy is represented by a classical scalar field  $\phi$  moving in a self-interaction potential  $V(\phi)$  and directly interacting with CDM particles through an exchange of energy-momentum, quantified by a coupling function  $\beta(\phi)$ . Here we will give only a very essential summary of the main features of cDE models, and we refer the reader to Amendola (2000); Baldi (2011b, 2012b) for a more thorough discussion.

The background dynamics of cDE cosmologies is described by the set of equations:

$$\dot{\rho}_r + 4H\rho_r = 0, \quad (1)$$

$$\dot{\rho}_b + 3H\rho_b = 0, \quad (2)$$

$$\dot{\rho}_c + 3H\rho_c = -\sqrt{\frac{2}{3}}\beta_c(\phi)\frac{\rho_c\dot{\phi}}{M_{Pl}}, \quad (3)$$

$$\ddot{\phi} + 3H\dot{\phi} + V'(\phi) = \sqrt{\frac{2}{3}}\beta_c(\phi)\frac{\rho_c}{M_{Pl}}, \quad (4)$$

where the subscripts  $r$ ,  $b$ ,  $c$  and  $\phi$ , indicate the energy densities  $\rho$  of

radiation, baryons, CDM, and the dark energy field  $\phi$ , respectively, and where the Hubble function is given as usual by

$$H^2 = \frac{8\pi G}{3} (\rho_r + \rho_c + \rho_b + \rho_\phi), \quad (5)$$

with  $M_{\bar{P}_i}^2 \equiv 1/8\pi G$  being the reduced Planck mass. In the above equations the field  $\phi$  is expressed in units of  $M_{\text{Pl}}$  and an overdot represents a derivative with respect to cosmic time while a prime denotes a derivative with respect to the field itself. The source terms on the right-hand side of Eqs. 3 and 4 define the interaction between the dark matter and the dark energy components, with a strength given by the coupling function  $\beta_c(\phi)$ .

At the level of linear density fluctuations, the interaction modifies the gravitational instability processes that govern the evolution of perturbations as a consequence of a long-range *fifth* force mediated by the dark energy field and acting between CDM fluid elements. In the Newtonian limit and on sub-horizon scales, these effects turn into the following set of modified linear equations (Amendola 2004; Pettorino & Baccigalupi 2008; Baldi 2012a):

$$\ddot{\delta}_c = -2H \left[ 1 - \beta_c \frac{\dot{\phi}}{\sqrt{6}H} \right] \dot{\delta}_c + 4\pi G [\bar{\rho}_b \delta_b + \bar{\rho}_c \delta_c \Gamma_c], \quad (6)$$

$$\ddot{\delta}_b = -2H \dot{\delta}_b + 4\pi G [\bar{\rho}_b \delta_b + \bar{\rho}_c \delta_c], \quad (7)$$

where  $\bar{\rho}_i$  represents the background density of the  $i$ -th fluid and  $\delta_i \equiv \delta\rho_i/\bar{\rho}_i$  its density perturbation. The factor  $\Gamma_c \equiv 1 + 4\beta_c^2/3$  represents the additional fifth force appearing only in the CDM equation while the term  $\beta_c \dot{\phi}$  is a velocity-dependent acceleration arising as a consequence of momentum conservation. Similar additional terms characterise the interaction among a discrete set of CDM particles in the non-linear regime (see Baldi et al. 2010).

## 2.2 The CoDECS simulations

For our investigation we will make use of the publicly available data of the CoDECS simulations (Baldi 2012b) that represent the largest suite of cDE simulations to date. These simulations are carried out with a suitably modified version of the TreePM N-body code GADGET (Springel 2005) that self-consistently implements all the above mentioned effects characterising cDE cosmologies (Baldi et al. 2010).

For the present work, we will employ the outputs of the L-CoDECS simulations, which follow the evolution of  $1024^3$  CDM particles and as many baryonic particles in a periodic cosmological box of 1 comoving Gpc/h a side. Both CDM and baryonic particles are treated as collisionless particles, but they experience different accelerations as a consequence of the interaction between the CDM and the dark energy fields.

The CoDECS suite includes six different cosmological models, for of them are considered in this paper: the reference  $\Lambda$ CDM cosmology, a cDE model (EXP003) characterised by a constant positive coupling  $\beta_c > 0$  and an exponential self-interaction potential of the form  $V(\phi) = A \exp(-\alpha\phi)$ , a further model (EXP008e3) with the same potential but with an exponential coupling,  $\beta_c(\phi) = \beta_0 \exp(\beta_1\phi)$ , and a final scenario (SUGRA003) with a constant negative coupling,  $\beta_c < 0$  and a SUGRA (Brax & Martin 1999) self-interaction potential  $V(\phi) = A\phi^{-\alpha} \exp(-\phi^2/2)$ . A summary of the models parameters is shown in Table 1. All the models have the same amplitude of perturbations at  $z = z_{\text{CMB}}$ , resulting in a different amplitude of linear density perturbations at the present epoch (and consequently different values of  $\sigma_8$ ).

In the present work we will also make use of the public

halo catalogs of the CoDECS simulations, that have been generated through a Friend-of-Friend (FoF) algorithm with a linking length of 0.2 times the mean inter-particle separation.

## 3 METHODOLOGY

We employ the publicly available void finder VIDE (Sutter et al. 2015c) to identify CV in the CDM and halo distributions extracted from the snapshots of the CoDECS simulations within the different cosmological models described above. VIDE embeds the ZOBOV algorithm, which allows to identify depressions in the density distribution of a set of points. In the following, we provide a very short summary of how ZOBOV works, and we refer to the original ZOBOV paper (Neyrinck 2008) for a more detailed discussion.

Firstly, ZOBOV associates a cell to each tracer (a CDM particle or a halo) using a Voronoi tessellation scheme, i.e. the cell  $c$  associated to the particle (or halo)  $p$  is defined as the region of the box which is closer to  $p$  than to any other particle (or halo) in the box. Secondly, the algorithm identifies local density minima among these cells: a density minimum is defined as a Voronoi cell with a lower density (i.e. a larger volume) than all other cells around it. Thirdly, ZOBOV joins together the Voronoi cells surrounding a local density minimum until cells with larger and larger density are found, and it identifies CV as the union of these cells. CV are joined together via the Watershed Transform (see Platen, van de Weygaert & Jones 2007), which naturally creates a hierarchy in the structures of CV. All these procedures are performed also by the ZOBOV version included in the VIDE toolkit. Additionally, VIDE provides several different void catalogs for which various types of sample selections (as e.g. different cuts on the void density contrast or on the void central overdensity) are applied on top of the original ZOBOV sample. In particular, as CV are found to define a complex hierarchy, with smaller voids being embedded in larger ones, VIDE provides for each identified void the corresponding hierarchy level, and according to this classification a sample of *main* CV (i.e. those CV that are not embedded in larger voids and that represent the top of their own void hierarchy) is produced. We employed a slightly modified version of this selection procedure (see Baldi et al. in prep.) to remove pathological CV from the catalog and obtain a more statistically robust and convergent sample of main CV.

Finally, since local density minima can also be found in overdense regions, we decide to remove from the main void catalogs the CV with a density minimum larger than 20% of the mean density of the Universe (which is one of the standard cuts provided by VIDE), in order to select only well defined CV for our comparisons. For each identified void, ZOBOV also calculates the probability that the void might arise in a uniform Poissonian distribution of points, which is directly related to the density contrast between the minimum density of the void and its boundary. As this density contrast is provided for each void also by the VIDE catalog, we remove CV with a density contrast below 1.57, corresponding to a probability of arising as Poisson noise larger than  $2\sigma$  (see Neyrinck 2008).

VIDE defines CV as spherical regions centered in the barycen-

**Table 1.** A summary of the cosmological models investigated in the present work and their main parameters. See Baldi (2012b) for details.

Model	Potential	$\alpha$	$\beta(\phi)$	$w_\phi(z=0)$	$\sigma_8(z=0)$
$\Lambda$ CDM	$V(\phi) = A$	–	–	–1.0	0.809
EXP003	$V(\phi) = Ae^{-\alpha\phi}$	0.08	0.15	–0.992	0.967
EXP008e3	$V(\phi) = Ae^{-\alpha\phi}$	0.08	$0.4 \exp[3\phi]$	–0.982	0.895
SUGRA003	$V(\phi) = A\phi^{-\alpha}e^{\phi^2/2}$	2.15	–0.15	–0.901	0.806

ter,  $\mathbf{x}_c$ , of the underdense regions provided by ZOBOV, where:

$$\mathbf{x}_c = \frac{\sum_{i=1}^N \mathbf{x}_i^p \cdot V_i^p}{\sum_{i=1}^N V_i^p}, \quad (8)$$

and  $\mathbf{x}_i^p$  and  $V_i$  are the positions of the  $i$ -th tracer and the volume of its associated Voronoi cell, while  $N$  is the number of tracers included in the void. The radius of the sphere (i.e. the effective radius of the void,  $R_{\text{eff}}$ ) is then computed from the overall volume of the underdense region by assuming sphericity:

$$V_{\text{VOID}} \equiv \sum_{i=1}^N V_i^p = \frac{4}{3} \pi R_{\text{eff}}^3. \quad (9)$$

It has been shown that different void finders based on dynamical criteria, instead of density or geometry criteria, might reduce the shot noise error (Elyiv et al. 2015). Nevertheless, the CV finder used here is accurate enough for the purpose of the present analysis, as we investigate the main properties of large CV extracted from dense numerical simulations.

#### 4 THE STATISTICS OF VOIDS IN THE CODECS

With the catalogs of CV extracted from the CoDECS simulations as described in the previous Section at hand, we perform some basic analyses of the statistical and structural properties of the CV in the different cosmologies, namely the CV filling factor (i.e. the fraction of the cosmic volume occupied by CV), their size distribution (i.e. the abundance of CV as a function of their size), and their stacked radial density profiles, and compare these observables to the reference  $\Lambda$ CDM case (see also Li 2011). We perform such comparison for CV identified both in a randomly subsampled CDM density field and in the distribution of collapsed halos, to highlight how the use of tracers with different bias might result in a different relative behaviour of the models.

##### 4.1 Void statistics in the CDM distribution

Let us start by considering the CV catalogs extracted from the CDM density field, i.e. directly from the CoDECS snapshots at different redshifts. To better handle the simulation data we have made use of the subsampling routine included in VIDE to randomly subsample the CDM particles of the simulation snapshots down to an average density of  $2 \times 10^7$  particles per cubic  $h^{-1} \text{Gpc}$ . For this comparison we will focus only on two out of the four models, namely the reference  $\Lambda$ CDM cosmology and the EXP003 scenario, which is the most extreme realisation (in terms of deviations at the background and linear perturbations level) of cDE models that we have at our disposal.

First of all, we compare the evolution of the volume fraction occupied by CV at different cosmic times, also known as the void filling factor, to check whether the interaction between DE and

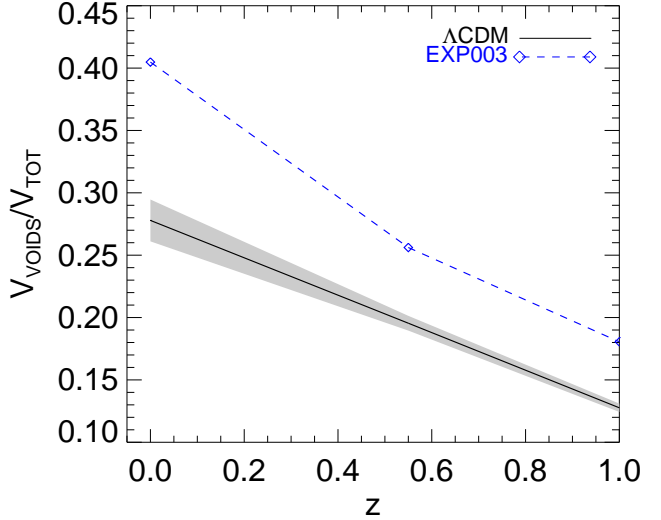


**Figure 1.** The redshift evolution of the volume fraction of CV identified in the CDM distribution for the  $\Lambda$ CDM (black solid line) and EXP003 (blue dashed line) models. The shaded area (shown only for  $\Lambda$ CDM) represents the uncertainty, computed with the jackknife method.

CDM particles implemented in our extreme cDE model has an impact on such fraction. Fig. 1 displays the evolution of the CV volume fraction,  $V_{\text{VOIDS}}/V_{\text{TOT}}$ , where  $V_{\text{VOIDS}}$  is the sum of all the main CV volumes in a given snapshot of the simulation and  $V_{\text{TOT}}$  is the total volume of the box, i.e.  $1 h^{-3} \text{Gpc}^3$ . The statistical error, shown in Fig. 1 by the shaded grey region around the  $\Lambda$ CDM line, has been computed with a jackknife method.

As expected, the volume fraction of CV increases with time, irrespectively of the underlying cosmological model, due to gravitational instability. Moreover, as one can see from Fig. 1, the volume fraction occupied by CV in the cDE model EXP003 is significantly larger than in the reference  $\Lambda$ CDM cosmology, reflecting the higher normalisation of the amplitude of linear perturbations at low redshifts in EXP003. More quantitatively, the volume fraction in EXP003 is roughly 40% larger than the corresponding  $\Lambda$ CDM fraction, at all redshifts between  $z = 1$  and  $z = 0$ . Clearly, the observed differences between the cDE model and the standard  $\Lambda$ CDM cosmology are statistically significant.

As a second step, we compare the relative abundance of CV as a function of their size, by computing in the two cosmological models the differential size distribution (hereafter DSD), defined as the number of CV with an effective radius  $R_{\text{eff}}$  falling within a set of size bins. In the upper panels of Fig. 2 we show the DSD at three different redshifts ( $z = \{0, 0.55, 1\}$ , from left to right) for the two cosmological models (black solid lines for  $\Lambda$ CDM and blue dashed lines for EXP003), while in the bottom panels we show the relative difference with respect to the reference  $\Lambda$ CDM cosmology (in units of its statistical error  $\sigma$ ). As one can see in the figure, at



$z = 0$  the number of CV in the cDE cosmology with  $R_{\text{eff}} \gtrsim 20 h^{-1} \text{Mpc}$  is at least 50% larger than in  $\Lambda\text{CDM}$ : this difference corresponds to more than  $4\sigma$ . At  $z = 0.55$  the same ratio applies to CV with  $R_{\text{eff}} \gtrsim 15 h^{-1} \text{Mpc}$ , and at  $z = 1$  to CV with  $R_{\text{eff}} \gtrsim 12 h^{-1} \text{Mpc}$ , with differences corresponding to  $5\sigma$  and  $7\sigma$ , respectively. Therefore, also in this different statistics the two models are clearly distinguishable from each other.

As a third statistic of our CV samples, we investigate the average stacked density profiles of CV having a comparable size. Many recent works (e.g. Ricciardelli, Quilis & Planelles 2013; Ricciardelli, Quilis & Varela 2014; Hamaus, Sutter & Wandelt 2014) suggested that the average profile of CV is self-similar in the standard  $\Lambda\text{CDM}$  cosmology, which makes CV an ideal target for geometrical tests such as the AP test. Therefore, we now aim at investigating whether the interaction between DE and CDM particles might induce some additional features on the density profile of CV.

To this end, we first compute the spherically-averaged radial density profile of each individual void by estimating the CDM density within a series of logarithmically equispaced spherical shells centred in the barycentre of each void and normalised to the void effective radius  $R_{\text{eff}}$ . The profiles are then stacked for CV with similar  $R_{\text{eff}}$ . Since the profiles of each void is calculated in units of  $R_{\text{eff}}$  in the first place, the stacking procedure basically consists in the calculation of the mean profile in each logarithmic radial bin. We randomly included 100 CV for each bin. The results are presented in Fig. 3, where we show the comparison of the stacked density profiles obtained using the CDM void catalog in the standard  $\Lambda\text{CDM}$  cosmology and in the EXP003 model. In the upper panels the error bars represent the corrected sample standard deviation computed on the 100 randomly selected CV. The shape of the profiles is qualitatively the same as found in previous works (Ricciardelli, Quilis & Planelles 2013; Ricciardelli, Quilis & Varela 2014; Hamaus, Sutter & Wandelt 2014): we observe a deep underdensity at  $R \rightarrow 0$  and a compensative overdensity at  $R \rightarrow R_{\text{eff}}$ . At  $R > 1.5 \cdot R_{\text{eff}}$  the profiles reach the mean density of the Universe. In the lower panels, we plot the relative difference between the models in units of the statistical significance  $\sigma$  computed as the sample standard deviation propagated to the relative difference. The grey shaded area represents a  $\pm 1\sigma$  significance.

As the figure clearly shows, the stacked profiles of EXP003 do not show significant differences from  $\Lambda\text{CDM}$  at the considered redshifts, with deviations always lying well within the mean square error. Nonetheless, we can observe that, at  $R \rightarrow 0$ , EXP003 generally shows a density 10 – 25% smaller than  $\Lambda\text{CDM}$ , thereby showing that CV are *emptier* in cDE. On the other hand, the compensative over-density at  $R = R_{\text{eff}}$  for EXP003 looks generally more prominent than  $\Lambda\text{CDM}$  (except for CV with  $5 < R_{\text{eff}} [h^{-1} \text{Mpc}] < 8$ ). Therefore, although with a low statistical significance, the central regions of the main CV appear to be more underdense in cDE models than in  $\Lambda\text{CDM}$ , which is expected to result in a corresponding stronger signal in void lensing surveys.

## 4.2 Void statistics in the halo distribution

We will now repeat the same three statistics of the CV properties discussed in Section 4.1 for the CV catalogs obtained by running VIDE on the distribution of FoF halos extracted from the CoDECS simulations at the same three redshifts investigated before (i.e.  $z = \{0, 0.55, 1\}$ ). The use of the FoF halos as tracers of the matter distribution has the appealing property to mimic real observations,

where CV are identified in the distribution of luminous galaxies. In particular, we have made use of the publicly available CoDECS halo catalogs that have been obtained through a FoF algorithm with a linking length 0.2 times the mean inter-particle separation. As we will show below, the differences between the cDE model EXP003 and the standard  $\Lambda\text{CDM}$  cosmology in all the three statistics are much weaker than what previously found for the CDM distribution. For this reason, we will include in this comparison also other two cDE models available within the CoDECS suite, namely the EXP008e3 and the SUGRA003 models (introduced in Section 2.2), in order to verify whether different realisations of the cDE scenario might have a stronger impact on the CV defined by the FoF halo distribution than the EXP003 model. Our comparison will show that this is actually not the case, as expected from the fact that EXP003 is the most extreme of the CoDECS models in terms of background and linear deviations from  $\Lambda\text{CDM}$ .

First of all, in Fig. 4 we compare the CV filling factor for these new void catalogs, as already done in Fig. 1 for the CV in the CDM distribution. The void volume and the dispersion indicated by the grey shaded area are computed as outlined above. The figure shows, as expected, that the void volume fraction increases in time, and that the  $\Lambda\text{CDM}$  model has generally the lowest volume fraction with respect to the other cDE models that are characterised by a higher normalisation of the linear power spectrum. Nonetheless, as the figure clearly shows, these differences are now much smaller and lie within the  $3\sigma$  statistical dispersion so that no significant differences in the CV filling factor appear among the various cDE models and the standard  $\Lambda\text{CDM}$  cosmology at all redshifts. This result is starkly different from what found for the CV in the CDM distribution for the EXP003 model.

In Fig. 5 we then display the DSD for CV identified in the distribution of FoF halos, analogously to what done in Fig. 2 for the CDM distribution. The DSD is shown for the different models ( $\Lambda\text{CDM}$  by black solid line, EXP003 by blue dashed line, EXP008e3 by orange dot-dashed line and SUGRA003 by red dotted line) in the upper panels, while the bottom panels report the percent deviation in units of the statistical significance  $\sigma$  from the reference  $\Lambda\text{CDM}$  case. While at  $z = 0$  and  $z = 0.55$  no significant differences appear among the models, one can observe an excess of small CV for the EXP003 model at  $z = 1$ . At this redshifts EXP003 shows  $\sim 50\%$  more CV with  $R_{\text{eff}} < 30 h^{-1} \text{Mpc}$  than  $\Lambda\text{CDM}$ , although within a confidence of  $1\sigma$ .

This is again a very different result with respect to what previously found for the CV identified in the CDM distribution, where the largest differences with respect to the standard cosmological model appeared at the large size tail of the distribution. It should however be noticed that due to the different density of the tracers between the subsampled CDM distribution adopted in the previous Section and the FoF halo distribution shown here, the mean separation between particles and hence the average size of CV is different in the two cases. Therefore, the size range that appeared as the large-size tail for the CDM CV ( $20 < R_{\text{eff}} [h^{-1} \text{Mpc}] < 30$ ) is now representing the small-size part of the void samples of the FoF halo distribution. For this reason, the two results might still appear consistent with each other despite their different qualitative trends. To address this issue, in Section 4.3 below we will compare the DSD of CV identified in a different random subsample of the CDM particles distribution with the same density of tracers as the FoF halo catalogue. Nonetheless, the clear differences between the background evolution of  $\Lambda\text{CDM}$  and cDE models (see Fig. 2) are not expected to be detected and do not appear for CV in halos.

Before moving to this additional comparison, we conclude

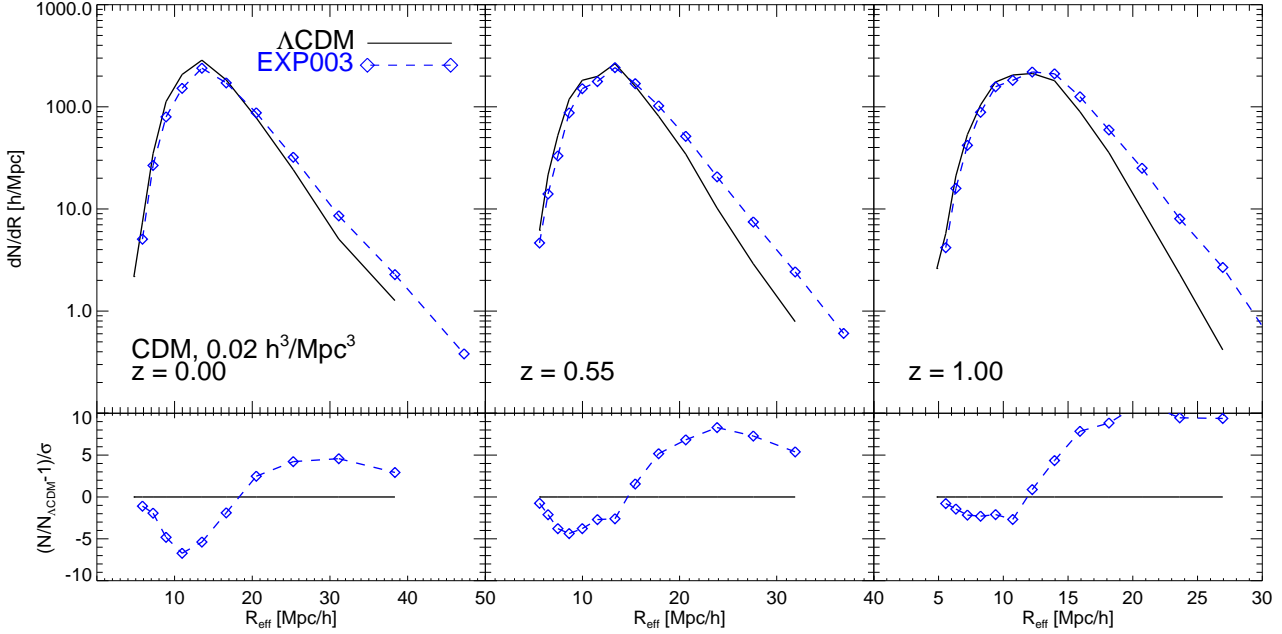


**Figure 2.** Top panels: the size distribution of CV in the CDM distribution for the  $\Lambda$ CDM (black solid line) and EXP003 (blue dashed lines) models. Bottom panels: the relative differences between the two models in units of the standard deviation  $\sigma$ , computed for the  $\Lambda$ CDM model.

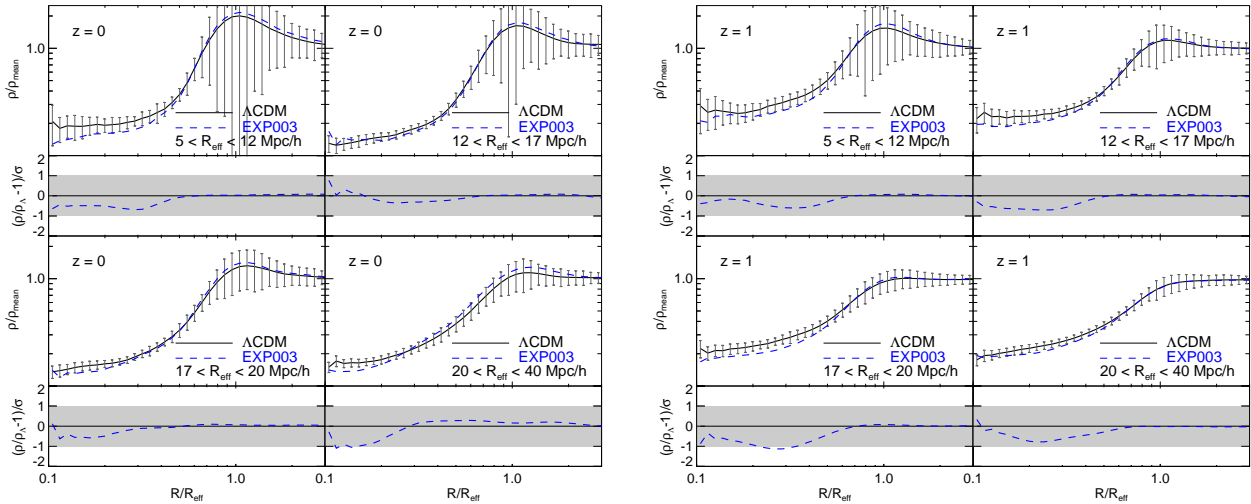


**Figure 3.** The stacked profiles of CV in the CDM distribution for the  $\Lambda$ CDM (black solid lines) and EXP003 (blue dashed lines) models. Results are displayed at two different redshifts,  $z = 0$  and  $z = 1$  (left and right blocks of panels, respectively) for four ranges of  $R_{\text{eff}}$ , as labeled. The error bars indicate the corrected sample standard deviation in each radial bin computed on the 100 randomly selected CV, while the sub-panels display the relative difference between the profiles in units of the statistical significance of the averaged profile.

our analysis of the CV extracted from the FoF halo distribution by comparing the void stacked density profiles as we did in Fig. 3 for the CV in the CDM distribution. In Fig. 6 we show the analogous to Fig. 3 for these new CV samples at  $z = 0$  and  $z = 1$ . For both redshifts we do observe significant deviations from the  $\Lambda$ CDM profile only in the inner part of the CV, where shot noise as well as an offset of the computed centre of the void from the real centre can strongly affect the profiles, as pointed out by e.g. Nadathur et al. (2015); Nadathur & Hotchkiss (2015). We also observe that the over-compensative region around  $\sim 1R_{\text{eff}}$  is not as

prominent as in the CDM CV (see Fig. 3), once again showing differences between tracers of density. We notice that the density minimum does not lie exactly at  $R \sim 0$ , which was not the case for CV in CDM. These last problem might be caused by the definition of centre as in eq. 8, as pointed out by Nadathur et al. (2015); Nadathur & Hotchkiss (2015). Eq. 8, anyway, is sufficient for our purpose because, by using it, we can easily compare our results with other works, and because we are not discussing features related to the correlation function of CV (in which the position of the centre of voids plays a fundamental role).

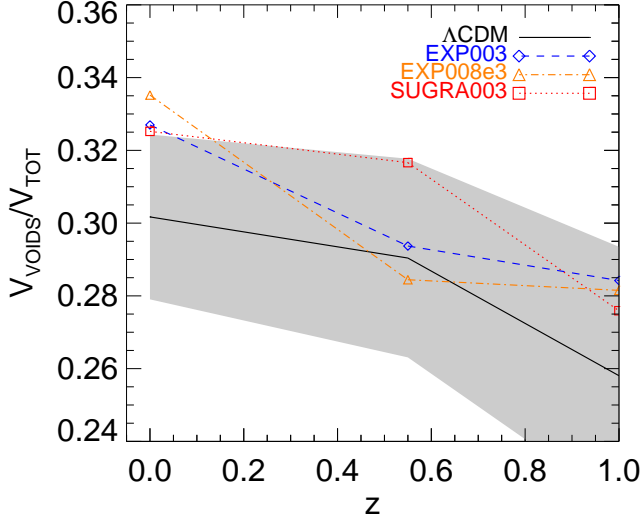


**Figure 4.** The redshift evolution of the volume fraction of CV identified in the halo distribution for different cosmological models:  $\Lambda$ CDM (black solid line), EXP003 (blue dashed line), EXP008e3 (dot-dashed orange line), SUGRA003 (red dotted line). The shaded area (shown only for  $\Lambda$ CDM) represents the uncertainty, computed with the jackknife method.

### 4.3 The impact of halo bias

As introduced in Section 4.2, it is interesting to compare the abundance of CV as a function of their effective radius,  $R_{\text{eff}}$ , for CV samples extracted from the FoF halo catalogs and from a random subsampling of the CDM distribution having the same number of tracers in the simulation box as the number of FoF halos. This will ensure that the mean inter-particle separation of the two samples of tracers is the same such that the corresponding average size of CV will be comparable in the two cases, thereby allowing for a direct comparison of the statistical properties of the two CV catalogs over a similar range of void sizes. This approach has been followed in several recent works (see e.g. Hamaus, Sutter & Wandelt 2014; Sutter et al. 2015b; Pisani et al. 2015), where the discriminating power of CV in future galaxy surveys has been inferred from the expected properties of CV identified in a random subsample of a simulated CDM distribution having the same density of the survey under investigation. To this end, we have randomly subsampled the CDM distribution of the CoDECS snapshots at the relevant redshifts to a total number of  $1.5 \cdot 10^6$  particles, corresponding to the total number of objects in the FoF halo catalog of the  $\Lambda$ CDM simulation at  $z = 0$ .

In Fig. 7 we show the equivalent to Fig. 2 for this new random subsampling and compare the abundance of CV in the  $\Lambda$ CDM and EXP003 models. We observe that, although the range of void sizes is now comparable to what was shown in Fig. 5, the comparison between  $\Lambda$ CDM and EXP003 still appears starkly different in the two cases. Also in this case, as already shown for a denser sample of CDM tracers, the EXP003 scenario includes a larger number of CV of large sizes at all redshifts with respect to the standard  $\Lambda$ CDM cosmology, with a qualitatively different trend with respect to what shown in Fig. 5. The comparison of Figs. 5 and 7 clearly indicates that CV in the CDM distribution and CV in the distribution of halos are characterised by different statistical properties. As the density of the two tracers is the same, these different properties

$z$	$\Lambda$ CDM			EXP003		
	$b$	$\sigma_8$	$b \cdot \sigma_8$	$b$	$\sigma_8$	$b \cdot \sigma_8$
0.00	1.2	0.809	0.971	1.046	0.967	1.011
0.55	1.584	0.618	0.979	1.310	0.733	0.960
1.00	2.049	0.504	1.033	1.633	0.595	0.972
1.60	2.903	0.398	1.155	2.235	0.468	1.046
2.00	3.630	0.348	1.263	2.739	0.408	1.118

**Table 2.** The bias  $b(z)$  and the normalisation of the linear perturbations amplitude  $\sigma_8(z)$  for the  $\Lambda$ CDM and EXP003 cosmologies. The rightmost column for each model displays the combination  $b(z) \cdot \sigma_8(z)$ , showing how this combination is much similar for the two models as compared to  $\sigma_8$  alone. As a consequence, the differences in the void populations extracted from the biased tracers within the two scenarios are significantly suppressed with respect to the case of the CV in the CDM distribution.

must be associated with the different bias of the two samples with respect to the underlying true density field: while a random subsampling of the CDM distribution is an unbiased tracer of the density field, halos are biased and the bias is expected to evolve differently in cDE models than in  $\Lambda$ CDM (Marulli, Baldi & Moscardini 2012; Moresco et al. 2014). More quantitatively, the lower bias of the EXP003 model compensates for the higher value of the perturbations amplitude. In Table 2 we display the value of the bias (as computed in Marulli, Baldi & Moscardini 2012) and of  $\sigma_8$  at various redshifts for the two models. As one can see from the last column, the combination  $b(z) \cdot \sigma_8(z)$  is substantially closer between the two models compared to the value of  $\sigma_8$  alone. This result suggests that the assumption (implicitly adopted in many recent works) that the properties of CV in a subsampled set of CDM particles extracted from a cosmological simulation can faithfully reproduce the statistics of CV identified in a galaxy survey is not valid.

In order to further validate this result, we compute the DSD of CV identified in the distribution of FoF halos with masses  $M > 5 \cdot 10^{12} M_{\odot}$ , thus considering tracers with larger masses and, therefore, with higher bias. This comparison is shown in the upper panels of Fig. 8, while the bottom panels display the deviation (in units of  $\sigma$ ) between the models. At  $z = 0$  we do not observe any significant difference between models (in agreement with Fig. 5), while at larger redshifts we find that the EXP003 cDE model features a larger number of small CV ( $30 < R_{\text{eff}}[h^{-1} \text{Mpc}] < 60$ ) as compared to  $\Lambda$ CDM, though the effect is small. The comparison between Figs. 2 and 8 indicates again that CV in the CDM distribution and in the distribution of halos are characterised by different statistical properties. This result clearly shows that the bias of the tracers from which CV are identified has a non-trivial impact on the relative statistical properties of the CV sample between two competing cosmological scenarios. Therefore, when comparing CV in  $\Lambda$ CDM and cDE models, CV in halos (which are biased tracers of the underlying density field) will not provide a faithful representation of how the models might differ in the properties of CV in the CDM distribution.

## 5 DISCUSSION AND CONCLUSIONS

In this paper we analysed the statistical properties of CV in  $\Lambda$ CDM and cDE models. In particular, we compared the properties of CV detected in the distribution of CDM and in collapsed halos, by means of a suite of large cosmological simulations, the CoDECS.

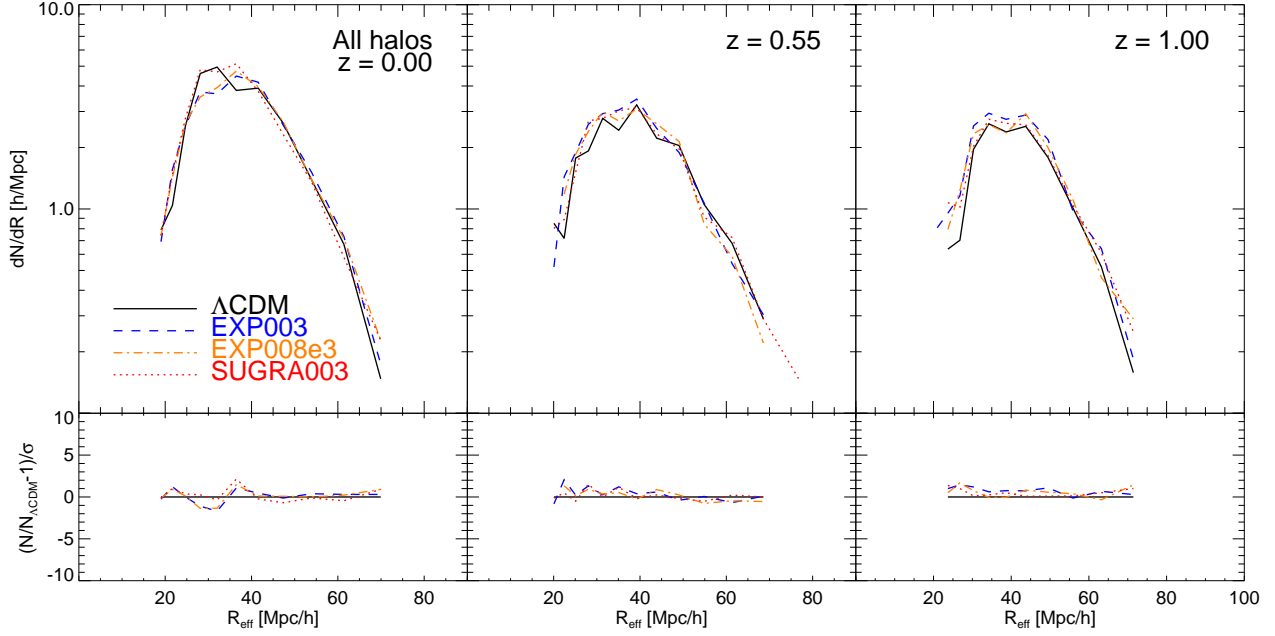


**Figure 5.** Top panels: the size distribution of CV in the halo distribution for the  $\Lambda$ CDM (black solid line), EXP003 (blue dashed lines), EXP008e3 (orange dot-dashed lines) and SUGRA003 (red dotted lines) models. Bottom panels: the relative differences between the cDE models and the  $\Lambda$ CDM one, in units of the standard deviation  $\sigma$ , computed for the  $\Lambda$ CDM model.

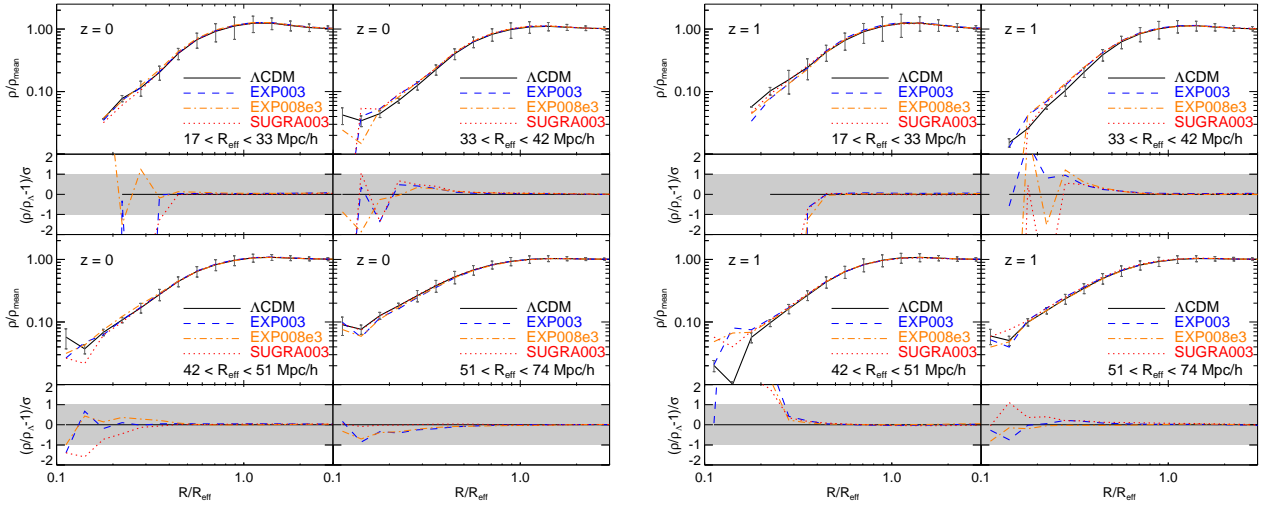


**Figure 6.** The stacked profiles of CV in the halo distribution for the  $\Lambda$ CDM (black solid lines), EXP003 (blue dashed lines), EXP008e3 (orange dot-dashed lines) and SUGRA003 (red dotted lines) models. Results are displayed at two different redshifts,  $z = 0$  and  $z = 1$  (left and right blocks of panels, respectively) for four ranges of  $R_{\text{eff}}$ , as labeled. The error bars in the upper panels are computed as for Fig. 3, and the sub-panels display again the relative difference of the profiles with respect to the  $\Lambda$ CDM one in units of the statistical significance of the averaged profile.

We focused on three CV statistics: the filling factor, the size distribution and the stacked density profiles.

In Section 4.1 we investigate the properties of CV in the CDM distribution, considering the  $\Lambda$ CDM and the cDE model EXP003, which represents – among the available CoDECS models – the most extreme case showing the largest discrepancies with respect to  $\Lambda$ CDM in several other observables (see e.g. the results of Baldi 2012b; Lee & Baldi 2011; Marulli, Baldi & Moscardini 2012; Beynon et al. 2012; Cui, Baldi & Borgani 2012; Giocoli et al.

2013; Carbone et al. 2013; Moresco et al. 2014; Pace et al. 2015; Giocoli et al. 2015). Our main results can be summarised as follows.

- (i) The filling factor of CV detected in the CDM distribution in the EXP003 model is significantly larger than in the  $\Lambda$ CDM case, as expected due to the higher normalization of the amplitude of linear perturbations at low redshift (Fig. 1). More quantitatively, the volume fraction in EXP003 is  $\sim 40\%$  larger than the corresponding



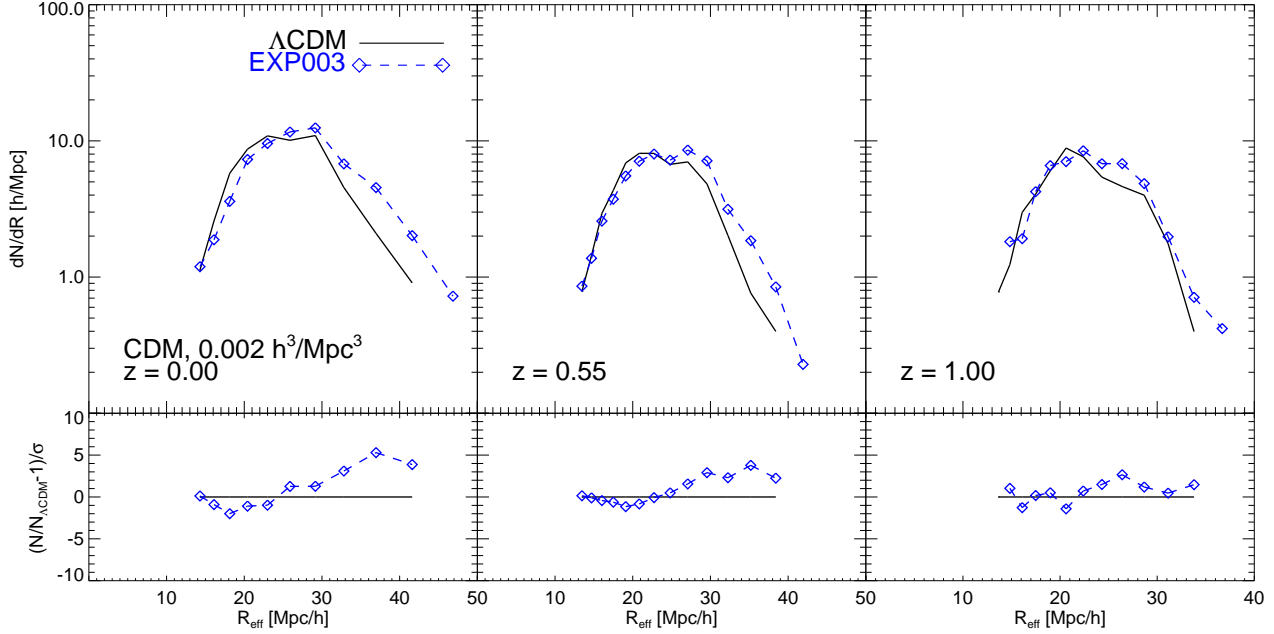


**Figure 7.** Top panels: the size distribution of CV in the CDM distribution diluted to the same density of the halo catalogue, for the  $\Lambda$ CDM (black solid lines) and EXP003 (blue dashed lines) models. Bottom panels: the relative differences between the two models, in units of the standard deviation,  $\sigma$ , computed for the  $\Lambda$ CDM model.

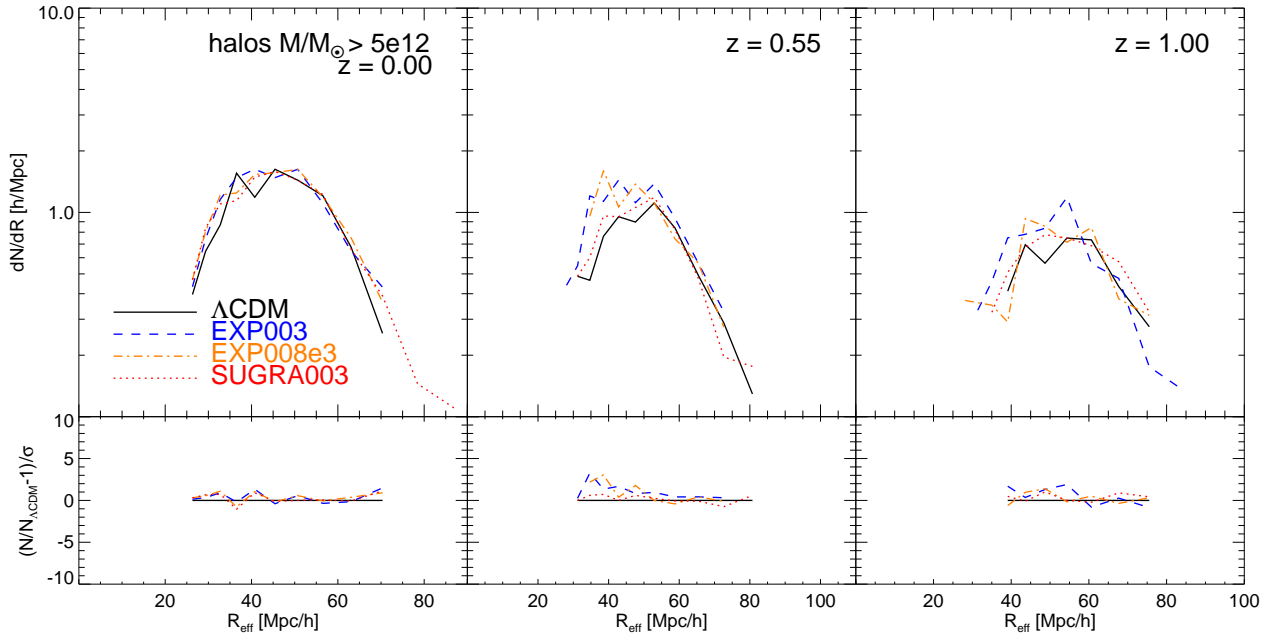


**Figure 8.** Top panels: the size distribution of CV identified in the distribution of halos with mass  $M > 5 \cdot 10^{12} M_{\odot}$ , for the  $\Lambda$ CDM (black solid lines), EXP003 (blue dashed lines), EXP008e3 (orange dot-dashed lines) and SUGRA003 (red dotted lines) models. Bottom panels: the relative differences between the cDE models and the  $\Lambda$ CDM one, in units of the standard deviation,  $\sigma$ , computed for the  $\Lambda$ CDM model.

$\Lambda$ CDM fraction: based on a jackknife approach, this is detectable with a very high statistical significance.

(ii) For what concerns the DSD (Fig. 2), we found an excess of large CV in the EXP003 model with respect to the reference  $\Lambda$ CDM cosmology, consistently with the general findings of Pisani et al. (2015). Quantitatively, the excess is around 50% with

a difference larger than  $4\sigma$ . The radius at which this excess starts to be significant decreases with redshift, being  $R \sim 20, 15, 12 h^{-1} \text{ Mpc}$  at  $z = 0, 0.55, 1$ , respectively.

(iii) The shape of the stacked density profile (Fig. 3) is qualitatively similar to what previously found in the literature (i.e density minima around the centres of the CV and overdense compensation

regions at  $R \sim R_{\text{eff}}$ ). The void profiles in cDE models are not significantly different from what observed in the standard cosmology. Nonetheless, we can observe that close to the CV centres, the EXP003 model generally displays a density 10 – 25% smaller than  $\Lambda$ CDM, thus showing that CV tend to be *emptier* in cDE models. On the other hand, the compensative overdensity at  $R \sim R_{\text{eff}}$  in the EXP003 case looks more prominent than in  $\Lambda$ CDM. All of these features are expected considering that the evolution of the background perturbations in cDE scenarios is faster than  $\Lambda$ CDM due to the *fifth force* associated with the coupling.

In Section 4.2 we then focused on CV identified in the halo distribution, finding that the comparison between cDE models and the reference cosmology is very different from what found for CDM. More specifically, we find the following results:

(i) The filling factor of CV in halos is not strongly dependent on the considered cDE model (Fig. 4). Only minor, not significant differences are found in the volume fractions at all redshifts considered in this paper. This last result is starkly different from what observed in CV samples detected in the CDM distribution.

(ii) The comparison of DSD (Fig. 5) in the halo distribution does not reveal sensible differences between cDE models and the reference one. This result is again substantially different from what found in Section 4.1. We connect this discrepancy with the impact of the halo bias on CV properties. To test such effect, we compare DSD of CV in a random subsample of the CDM distribution with the same density of tracers as the FoF halo catalog. Again, in this last case CV in CDM do not show the same relative trend in the DSD as for the CV in the halo distribution (Fig. 7). The impact of the halo bias can be observed also by increasing the minimum mass of halos used as tracers: in Fig. 8 we show that including only halos with large masses ( $> 5 \cdot 10^{12} \cdot M_{\odot}$ ) the cDE models show an excess of CV with  $30 < R_{\text{eff}} [h^{-1} \text{Mpc}] < 60$  at  $z = 0.55, 1$ , which is not seen in Fig. 5.

(iii) The density profile of CV in halos does not look like an effective probe to discriminate among cDE models. Indeed, as shown in Fig. 6, the stacked profiles of CV in cDE models are only marginally distinguishable from the  $\Lambda$ CDM case, and only in the very innermost parts.

To conclude, the main result of this work is that the properties of CV in different cosmological models are strongly affected by the choice of the tracers of the underlying density field used to detect them (halos or CDM particles): this is caused by the impact of the halo bias on the structural properties of CV: as the bias evolves differently for different cDE models, this is reflected in a non-trivial way on the properties of the associated CV sample. Our results indirectly challenge the assumption made in several recent works that a subsampled distribution of simulated CDM particles with the same density of the expected tracers of a real galaxy survey might provide reliable predictions about the effective discriminating power of CV in that survey.

## ACKNOWLEDGMENTS

We are thankful to Gianni Zamorani for useful hints on the statistical comparison between the models. GP would like to thank Jochen Weller and Ben Hoyle for useful suggestions and Paul Sutter for helpful discussions about ZOBOV and VIDE. The numerical simulations presented in this work have been performed and analysed on the Hydra cluster at the RZG supercomputing centre

in Garching. MB acknowledges support by the Marie Curie Intra European Fellowship “SIDUN” within the 7th Framework Programme of the European Commission. We acknowledge financial contributions from contracts ASI/INAF I/023/12/0 and by the PRIN MIUR 2010-2011 “The dark Universe and the cosmic evolution of baryons: from current surveys to Euclid”. MB and LM also acknowledge the financial contribution by the PRIN INAF 2012 “The Universe in the box: multiscale simulations of cosmic structure”.

## REFERENCES

- Alcock C., Paczynski B., 1979, *Nature*, 281, 358  
 Amendola L., 2000, *Phys. Rev.*, D62, 043511  
 Amendola L., 2004, *Phys. Rev.*, D69, 103524  
 Amendola L., 2004, *Phys. Rev. D*, 69, 103524  
 Amendola L., et al., 2013, *Living Reviews in Relativity*, 16, 6  
 Baldi M., 2011a, *MNRAS*, 414, 116  
 Baldi M., 2011b, *MNRAS*, 411, 1077  
 Baldi M., 2012a, *MNRAS*, 420, 430  
 Baldi M., 2012b, *MNRAS*, 422, 1028  
 Baldi M., 2012c, *MNRAS*, 422, 1028  
 Baldi M., Pettorino V., Robbers G., Springel V., 2010, *MNRAS*, 403, 1684  
 Beynon E., Baldi M., Bacon D. J., Koyama K., Sabiu C., 2012, *Mon.Not.Roy.Astron.Soc.*, 422, 3546  
 Bos E. G. P., van de Weygaert R., Dolag K., Pettorino V., 2012, *MNRAS*, 426, 440  
 Boylan-Kolchin M., Bullock J. S., Kaplinghat M., 2011, *MNRAS*, 415, L40  
 Brax P. H., Martin J., 1999, *Physics Letters B*, 468, 40  
 Bullock J. S., 2010, *ArXiv e-prints*  
 Carbone C., Baldi M., Pettorino V., Baccigalupi C., 2013, *JCAP*, 1309, 004  
 Carlesi E., Knebe A., Lewis G. F., Wales S., Yepes G., 2014a, *MNRAS*, 439, 2943  
 Carlesi E., Knebe A., Lewis G. F., Yepes G., 2014b, *MNRAS*, 439, 2958  
 Cervantes V. D. V., Marulli F., Moscardini L., Baldi M., Cimatti A., 2012, *ArXiv e-prints*  
 Clampitt J., Cai Y.-C., Li B., 2013, *MNRAS*, 431, 749  
 Clampitt J., Jain B., 2014, *ArXiv e-prints*  
 Colberg J. M., Sheth R. K., Diaferio A., Gao L., Yoshida N., 2005, *MNRAS*, 360, 216  
 Cui W., Baldi M., Borgani S., 2012, *arXiv:1201.3568*  
 D’Amico G., Musso M., Noreña J., Paranjape A., 2011, *Phys. Rev. D*, 83, 023521  
 de Blok W. J. G., 2010, *Advances in Astronomy*, 2010, 5  
 Elyiv A., Marulli F., Pollina G., Baldi M., Branchini E., Cimatti A., Moscardini L., 2015, *MNRAS*, 448, 642  
 Farrar G. R., Peebles P. J. E., 2004, *ApJ*, 604, 1  
 Finelli F., Garcia-Bellido J., Kovacs A., Paci F., Szapudi I., 2014, *ArXiv e-prints*  
 Gibbons G. W., Werner M. C., Yoshida N., Chon S., 2014, *MNRAS*, 438, 1603  
 Giocoli C., Marulli F., Baldi M., Moscardini L., Metcalf R. B., 2013, *arXiv:1301.3151*  
 Giocoli C., Metcalf R. B., Baldi M., Meneghetti M., Moscardini L., et al., 2015  
 Gregory S. A., Thompson L. A., Tift W. G., 1978, in *Bulletin of the American Astronomical Society*, Vol. 10, *Bulletin of the American Astronomical Society*, p. 622

- Hamaus N., Sutter P. M., Wandelt B. D., 2014, *Physical Review Letters*, 112, 251302
- Hausman M. A., Olson D. W., Roth B. D., 1983, *ApJ*, 270, 351
- Izumi K., Hagiwara C., Nakajima K., Kitamura T., Asada H., 2013, *Phys. Rev. D*, 88, 024049
- Kirshner R. P., Oemler, Jr. A., Schechter P. L., Sackett P. C., 1981, *ApJ*, 248, L57
- Kovač K. et al., 2014, *MNRAS*, 438, 717
- Krause E., Chang T.-C., Doré O., Umetsu K., 2013, *ApJ*, 762, L20
- Laureijs R., et al., 2011, *ArXiv e-prints*
- Lavaux G., Wandelt B. D., 2010, *MNRAS*, 403, 1392
- Lee J., Baldi M., 2011, *ApJ* in press, arXiv:1110.0015, *ApJ* Submitted
- Li B., 2011, *Mon.Not.Roy.Astron.Soc.*, 411, 2615
- Li B., Barrow J. D., 2011, *Phys. Rev.*, D83, 024007
- Li B., Zhao H., 2009, *Phys. Rev. D*, 80, 044027
- Macciò A. V., Quercellini C., Mainini R., Amendola L., Bonometto S. A., 2004, *Phys. Rev.*, D69, 123516
- Marulli F., Baldi M., Moscardini L., 2012, *MNRAS*, 420, 2377
- Melchior P., Sutter P. M., Sheldon E. S., Krause E., Wandelt B. D., 2014, *MNRAS*, 440, 2922
- Moresco M., Marulli F., Baldi M., Moscardini L., Cimatti A., 2014, *MNRAS*, 443, 2874
- Nadathur S., Hotchkiss S., 2015, *ArXiv e-prints*
- Nadathur S., Hotchkiss S., Diego J. M., Iliev I. T., Gottlöber S., Watson W. A., Yepes G., 2015, *MNRAS*, 449, 3997
- Neyrinck M. C., 2008, *MNRAS*, 386, 2101
- Nusser A., Gubser S. S., Peebles P. J., 2005, *Phys. Rev. D*, 71, 083505
- Odrzywólek A., 2009, *Phys. Rev. D*, 80, 103515
- Pace F., Baldi M., Moscardini L., Bacon D., Crittenden R., 2015, *MNRAS*, 447, 858
- Peebles P. J. E., 2001, *ApJ*, 557, 495
- Pettorino V., Baccigalupi C., 2008, *Phys. Rev. D*, 77, 103003
- Pisani A., Sutter P. M., Hamaus N., Alizadeh E., Biswas R., Wandelt B. D., Hirata C. M., 2015, *ArXiv e-prints*
- Planck Collaboration et al., 2015a, *ArXiv e-prints*
- Planck Collaboration et al., 2015b, *ArXiv e-prints*
- Platen E., van de Weygaert R., Jones B. J. T., 2007, *MNRAS*, 380, 551
- Ratra B., Peebles P. J. E., 1988, *Phys. Rev. D*, 37, 3406
- Rees M. J., Sciama D. W., Stobbs S. H., 1968, *Astrophys. Lett.*, 2, 243
- Ricciardelli E., Quilis V., Planelles S., 2013, *MNRAS*, 434, 1192
- Ricciardelli E., Quilis V., Varela J., 2014, *MNRAS*, 440, 601
- Spolyar D., Sahlén M., Silk J., 2013, *Physical Review Letters*, 111, 241103
- Springel V., 2005, *Mon. Not. Roy. Astron. Soc.*, 364, 1105
- Sutter P. M., Carlesi E., Wandelt B. D., Knebe A., 2015a, *MNRAS*, 446, L1
- Sutter P. M., Carlesi E., Wandelt B. D., Knebe A., 2015b, *MNRAS*, 446, L1
- Sutter P. M. et al., 2015c, *Astronomy and Computing*, 9, 1
- Sutter P. M., Lavaux G., Wandelt B. D., Weinberg D. H., 2012, *ApJ*, 761, 187
- Sutter P. M., Pisani A., Wandelt B. D., Weinberg D. H., 2014, *MNRAS*, 443, 2983
- Szapudi I. et al., 2014, *ArXiv e-prints*
- Tinker J. L., Conroy C., 2009, *ApJ*, 691, 633
- Weinberg S., 1989, *Reviews of Modern Physics*, 61, 1
- Wetterich C., 1988, *Nuclear Physics B*, 302, 668
- Wetterich C., 1995, *Astron. Astrophys.*, 301, 321